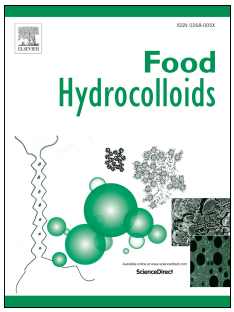

Enhanced structural properties of calcium cross-linked pectin gel beads incorporated with starch derivatives: Preparation, characterization, and *in vitro* prebiotic activity

Wenqing Zhu, Ruoxi Bai, Shulei Liang, Yuqin Yuan, Bin Zhang, Marie-Laure Fauconnier, Aurore Richel, Zhenjia Zheng

PII: S0268-005X(25)01146-4

DOI: https://doi.org/10.1016/j.foodhyd.2025.112186

Reference: FOOHYD 112186

To appear in: *Food Hydrocolloids*

Received Date: 6 August 2025

Revised Date: 28 October 2025

Accepted Date: 29 October 2025

Please cite this article as: Zhu, W., Bai, R., Liang, S., Yuan, Y., Zhang, B., Fauconnier, M.-L., Richel, A., Zheng, Z., Enhanced structural properties of calcium cross-linked pectin gel beads incorporated with starch derivatives: Preparation, characterization, and *in vitro* prebiotic activity, *Food Hydrocolloids*, https://doi.org/10.1016/j.foodhyd.2025.112186.

Preparation method

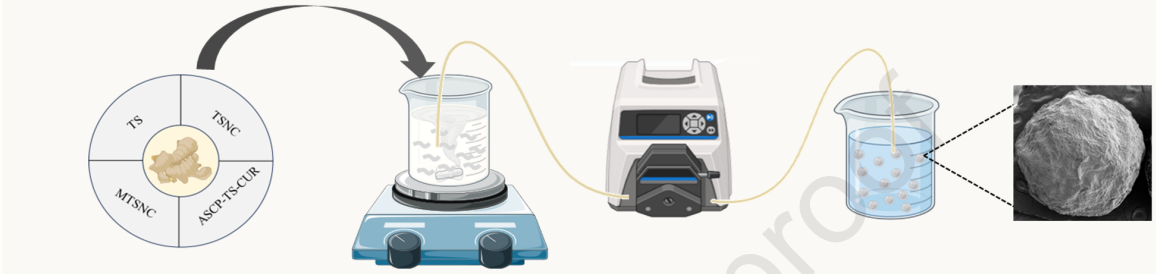

Structural and functional characteristics

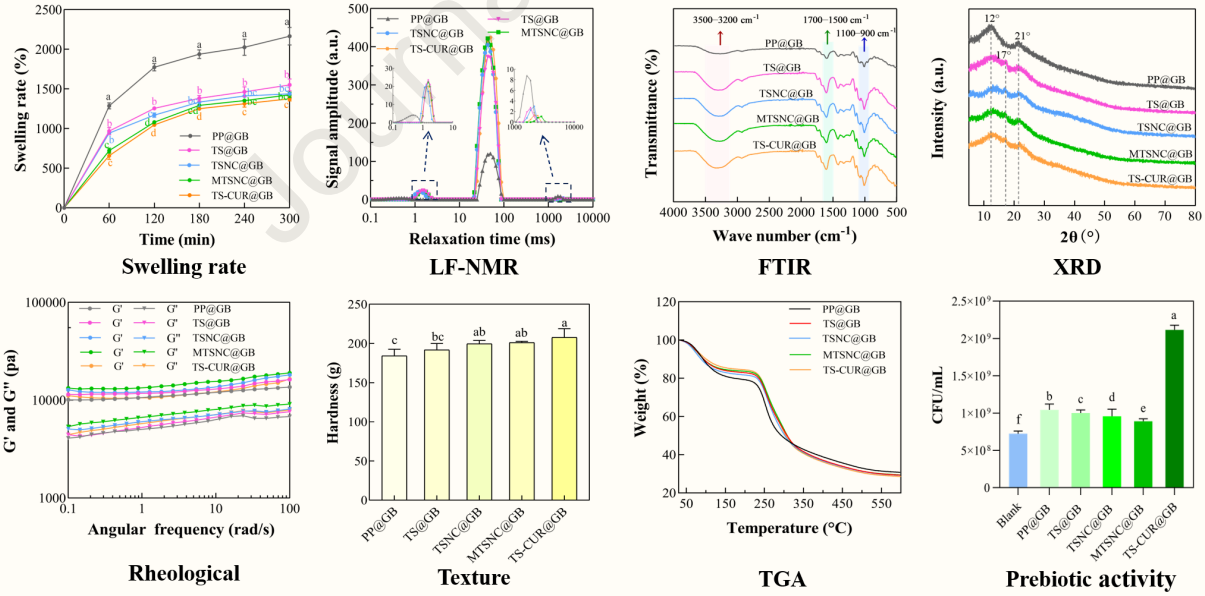

Enhanced structural properties of calcium cross-linked pectin gel beads incorporated with starch derivatives: Preparation, characterization, and *in vitro* prebiotic activity

Wenqing Zhu[a,b], Ruoxi Bai[a], Shulei Liang[a], Yuqin Yuan[a], Bin Zhang[a], Marie-Laure Fauconnier[b], Aurore Richel[c], Zhenjia Zheng[a,*]

[a] Key Laboratory of Food Nutrition and Health in Universities of Shandong, College of Food Science and Engineering, Shandong Agricultural University, 61 Daizong Street, Tai'an 271018, Shandong, China

[b] Laboratory of Chemistry of Natural Molecules, Gembloux Agro-Bio Tech, University of Liège, Passage des déportés 2, B-5030 Gembloux, Belgium

[c] Laboratory of Biomass and Green Technologies, Gembloux Agro-Bio Tech, University of Liège, Passage des déportés 2, B-5030 Gembloux, Belgium

[*] Corresponding author: Zhenjia Zheng (Email: zhengzhenjia@sdau.edu.cn)

Abstract: In this study, gel beads composed of pectin and four different starch-based derivatives were prepared through calcium ion crosslinking, and their physicochemical characteristics and functional properties were systematically evaluated. The results indicated that the incorporation of starch derivatives increased the internal crosslinking degree and strengthened intermolecular interactions, leading to a more compact and densely arranged porous structure within the composite gel beads. Compared to pure pectin gel beads, the water holding capacity of the composite gel beads improved by 6.06%–15.44% while the swelling rate decreased by 26.16%–37.02%, and the hardness, springiness, chewiness, and gumminess increased by 4.16%–12.75%, 3.40%–4.96%, 1.71%–8.63%, and 8.09%–16.51%, respectively. Additionally, the incorporation of starch derivatives reduced the crystallinity of the composite gel beads and enhanced their thermal stability. Moreover, all five gel beads exhibited notable prebiotic activity, significantly promoting the growth of *Lactiplantibacillus plantarum* Lp3a. Notably, the gel beads incorporating starch-curcumin complexes (TS-CUR@GB) achieved the highest colony count of 2.15×10^9 CFU/mL, which was 2.92-fold higher than the blank group. These results demonstrate the potential of starch-based derivatives to improve the structural integrity and functional performance of pectin-based gel systems, offering promising applications in food science and bioactive delivery systems.

Keywords: Pectin, starch derivatives, gel beads, structural analysis, physicochemical properties, *in vitro* prebiotic activity

1. Introduction

Hydrogels are three-dimensional networks of hydrophilic polymers, such as sodium alginate, pectin, that can absorb and retain large amounts of water or other substances. Their excellent biocompatibility and environmental friendliness have sparked widespread interest in the fields of food science and biomedicine (Yang et al., 2024). Among various hydrogel configurations, hydrogel beads have gained widespread application due to their small size and spherical morphology, which facilitates easy incorporation into food matrices. Moreover, the three-dimensional gel network provides a protective barrier that stabilizes sensitive bioactive compounds and protects them from adverse external conditions, thereby enabling their extensive use in the encapsulation, protection, and controlled release of functional ingredients (Li et al., 2024). A common method for producing gel beads is ionic gelation, in which divalent cations (e.g., Ca^{2+}) cross-link charged hydrocolloids to form a stable three-dimensional polymeric network (Almeida et al., 2021). Low-methoxy pectin is especially suitable for this process due to its non-toxicity, biocompatibility, and ability to rapidly form a stable “egg-box” gel structure upon calcium cross-linking (Lenie et al., 2024). Nevertheless, pure pectin gel beads often exhibit certain structural limitations, such as high porosity, a loosely structured network, and excessive swelling behavior, which can lead to poor encapsulation efficiency and premature release of bioactive components (Silveira et al., 2023).

To address these structural limitations, researchers have explored the integration of various filler materials, including sodium alginate (Zhang et al., 2025), starch (Silveira et al., 2023), chitosan (Reichembach et al., 2024), and proteins (Sun et al., 2024) to reinforce the hydrogel network and enhance functional performance. Among them, starch, one of the most abundant and important natural polysaccharides, is considered a promising sustainable biomaterial due to its complete biodegradability, low cost, and renewability (Wang et al., 2025). It has been widely used in the food industry as a thickening agent, stabilizer, gelling agent, and water-retaining agent to improve textural properties, viscoelasticity, and overall stability of food products (Ren, Jiang, et al., 2020). Furthermore, native starch has been successfully incorporated into

the ionic gelation process as a filler matrix to enhance the swelling behavior and structural characteristics of hydrogel beads (Lopes et al., 2023). For instance, Chan et al. (2011) reported that corn starch not only enhances the structural characteristics of alginate-based gel beads but also significantly improves the viability of *Lactobacillus casei* during storage. Rohman et al. (2021) demonstrated that cassava starch acts as an effective filler, improving the morphological features and encapsulation efficiency of alginate hydrogels. Furthermore, corn starch fillers can reduce the swelling phenomenon of the gel network and further enhance its mechanical properties (Chen et al., 2024). However, the current research primarily focuses on the application of natural starch as a structural regulator, while the regulating potential of starch derivatives with progressively enhanced structures and functions on the properties of pectin-based gel beads has not been explored.

We hypothesized that each structurally progressive starch system would enhance the mechanical strength, swelling resistance, and thermal stability of gel beads through differentially modulating the cross-linking density and network architecture, especially those pre-loaded with bioactive components (such as curcumin), which can not only improve the structural defects but also endow gel beads with biological function benefits. To prove our hypothesis, this study aims to develop a series of pectin-based gel beads that contain four starch-based derivatives (natural starch, starch nanoparticles, modified starch nanoparticles, and starch-curcumin complexes), simulating the gradual evolution of starch structure from natural form to nanoscale, modified state, and functionalized complexes. Subsequently, a systematic evaluation was conducted on the microstructure, mechanical properties, swelling behavior, and prebiotic activity of these gel beads, aiming to clarify the regulatory effect of the structural and functional evolution of starch fillers on the overall performance of pure pectin gel beads, while providing valuable insights for the design and development of novel hydrogel systems with enhanced structure and functionality.

2. Materials and methods

2.1. Materials and chemicals

Pectin (food grade, apple-derived, APA210) was supplied by Yantai DSM Andeli

Pectin Co., Ltd. The galacturonic acid (GalA) content of this pectin is 85.6%, the degree of esterification (DE) is 27.9%, and the weight-average molecular weight (Mw) is 161352 ± 6460 Da. Calcium chloride (food grade) was purchased from Shenzhen Xingmu Bioengineering Co., Ltd. Turmeric starch (starch content 80.85%, moisture content 13.15%, fat content 0.10%, protein content 0.15%, ash content 0.80%, amylose content 55.06%) was extracted from turmeric rhizomes using the method described in our previous study (Zhu et al., 2025), in which its structural characteristics were comprehensively analyzed. All other reagents were of analytical grade.

2.2. Synthesis of starch-based derivatives

The synthesis of starch-based derivatives was carried out as described in our previous study (Zhu et al., 2025).

Starch nanoparticles were synthesized using the antisolvent precipitation method. Briefly, turmeric starch (TS) was gelatinized and added to an antisolvent (anhydrous ethanol) under continuous stirring. The mixture was then regenerated at 4°C for 24 h, followed by centrifugation at 4000 rpm for 10 min. The resulting precipitate was collected, washed, and then subjected to freeze-drying, yielding a powdered sample named TSNC.

Modified starch nanoparticles, named MTSNC, were prepared by incorporating dioscin during the synthesis process. Specifically, anhydrous ethanol containing dioscin was added to the turmeric starch gelatinization solution. Subsequently, the remaining steps were carried out in the same manner as for TSNC.

The dioscin-modified turmeric starch-curcumin complex, named ASCP-TS-CUR, was synthesized using the antisolvent co-precipitation (ASCP) method. The detailed procedure has been reported in the referenced publication.

2.3. Preparation of pectin-based gel beads filled with different starch derivatives

The preparation of pectin-based gel beads incorporating various starch-based derivatives was conducted following the procedures described by Jiang et al. (2024) and Dahal et al. (2024), with slight modifications. In brief, 1.0 g of each starch-based derivative (TS, TSNC, MTSNC, and ASCP-TS-CUR) was dispersed into a 5% (*w/v*) pectin solution and stirred continuously for 30 min to ensure thorough mixing. The

resulting mixture was then inhaled into a peristaltic pump and extruded dropwise into a 4% (*w/v*) $CaCl_2$ crosslinking solution under gentle stirring for 30 min to facilitate curing. The formed gel beads were subsequently collected, rinsed three times with deionized water to remove excess Ca^{2+}, and freeze-dried (–80°C, 10 Pa) for 12 hours to obtain the final dried products. The pectin gel beads containing TS, TSNC, MTSNC, and ASCP-TS-CUR were designated as TS@GB, TSNC@GB, MTSNC@GB, and TS-CUR@GB, respectively. For comparison, pure pectin gel beads without any starch-based materials were prepared using the same procedure and designated as PP@GB.

2.4. Appearance observation

The morphological characteristics and overall appearance of both fresh and freeze-dried gel beads were observed and captured using a smartphone (OnePlus Ace 2, PHK110).

2.5. Fourier transform infrared (FTIR) spectroscopy analysis

The chemical structure and functional groups of the dried gel beads were analyzed using a Nicolet iS10 Fourier Transform Infrared (FTIR) spectrometer (Thermo Fisher Scientific, USA), following the method described by Reichembach et al. (2024). The spectra were recorded over a wavelength range of 4000 to 400 cm^{-1} with a resolution of 4 cm^{-1} and 64 scans.

2.6. X-ray diffraction (XRD) analysis

The crystallographic properties of the dried gel bead samples were determined using an EMPYREAN X-ray diffractometer (Malvern Panaco Instruments LTD., UK) equipped with a Cu-Kα radiation source. The diffractometer was operated at an acceleration voltage of 40 kV and a current of 40 mA. The diffraction patterns were recorded across a 2θ range of 5° to 80° with a scanning rate of 10°/min, following the procedure described by Lee et al. (2020).

2.7. Thermogravimetric analysis (TGA)

The thermogravimetric behavior of the dried gel bead samples was analyzed using a D-09123 thermogravimetric analyzer (Mettler Toledo Instruments Ltd., Zurich, Switzerland), following the method described by Bu et al. (2023). Each sample was heated from 30°C to 600°C at a heating rate of 10°C/min. All measurements were

conducted in a nitrogen atmosphere, with a continuous flow rate of 30 mL/min.

2.8. Scanning electron microscope (SEM) analysis

The surface and cross-sectional morphologies of the dried gel beads were examined using a SUPRA 55 scanning electron microscope (Carl Zeiss Group, Germany), following the procedure described by Cai et al. (2022). Briefly, approximately 10 mg of dried gel bead samples were mounted onto the observation table and sputter-coated with a thin layer of gold. The microstructural features were then observed under an accelerating voltage of 10 kV.

2.9. Water holding capacity (WHC)

The WHC of the gel beads was determined according to the method described by Feltre et al. (2020). Briefly, freshly prepared gel beads were weighed to record their initial mass. The beads were then placed into centrifuge tubes and centrifuged at 4000 rpm for 20 min. Following centrifugation, the residual gel beads were reweighed. The WHC was calculated using Eq. (1):

$$WHC\ (\%) = \frac{Mass\ of\ gel\ beads\ after\ centrifugation}{Mass\ of\ gel\ beads\ before\ centrifugation} \times 100 \quad (1)$$

2.10. Swelling rate (SR) analysis

The swelling behavior of the dried gel beads over 6 hours was evaluated following the method of Cai et al. (2022), with slight modifications. Briefly, approximately 50 mg of freeze-dried gel beads were immersed in 20 mL of deionized water at room temperature. At predetermined time intervals (60, 120, 180, 240, 300, and 360 min), the swollen beads were retrieved, gently blotted with filter paper to remove excess surface water, and immediately weighed. The SR was calculated using Eq. (2):

$$SR\ (\%) = \frac{Weight\ of\ swollen\ gel\ beads - Weight\ of\ dried\ gel\ beads}{Weight\ of\ dried\ gel\ beads} \times 100 \quad (2)$$

2.11. Low-field nuclear magnetic resonance (LF-NMR) analysis

The water distribution within the gel beads was analyzed using a low-field nuclear magnetic resonance (LF-NMR) spectrometer (Niumag Analytical Instrument Corporation, China), following the method described by Jiang et al. (2024). Before measurement, approximately 1 g of freshly prepared gel beads was placed into an NMR tube and inserted into the sample chamber of the LF-NMR instrument. The transverse

relaxation time (T_2) was measured using the Carr-Purcell-Meiboom-Gill (CPMG) pulse sequence with a superposition number (NS) of 4, an echo time (TE) of 0.25 ms, and an echo number (NECH) of 18000. The obtained T_2 relaxation curves were analyzed through multi-exponential fitting to quantify the relative proportions of different water populations within the gel matrix.

2.12. Rheological analysis

According to the method described by Zhang et al. (2025), the rheological behavior of the fresh gel beads was evaluated at 25°C using an MCR102 Modular Intelligent Rheometer (Anton Paar Instruments Co. Ltd., Austria) equipped with a parallel plate geometry (diameter of 40 mm, gap height of 1 mm). Specifically, an appropriate amount of fresh gel beads was loaded onto the lower plate, and a layer of silicone oil was coated around the samples to prevent slippage and water evaporation. Dynamic oscillatory frequency sweeps were performed over a frequency range of 0.1 to 100 rad/s under a constant strain of 0.5%, and the storage modulus (G′) and loss modulus (G″) were recorded as functions of angular frequency to assess the viscoelastic properties of the samples. The G′ and G″ curves obtained from frequency sweep data were modeled from 0.1 to 100 rad/s using a power law as defined in Eq. (3) and Eq. (4).

$$G' = k' \times \omega^{n'} \qquad (3)$$

$$G'' = k'' \times \omega^{n''} \qquad (4)$$

where ω is the frequency (rad/s), G′ is the storage modulus at the given frequency, G″ is the loss modulus at the given frequency, k′ is the elastic stiffness coefficient ($Pa \cdot s^n$), k″ is the viscosity stiffness coefficient ($Pa \cdot s^n$), n′ is the elastic frequency index (dimensionless), n″ is the viscosity frequency index (dimensionless). Additionally, k″/k′ represents the overall loss tangent.

The steady-state scanning shear rate was 0.1 to 100 s^{-1}, and the viscosity was recorded as a function of the shear rate. The viscosity curve was fitted and analyzed using the Ostwald-de Wael power-law model defined in Eq. (5).

$$\eta_a = K \times \dot{\gamma}^{n-1} \qquad (5)$$

where η_a is the apparent viscosity (Pa·s), K is the consistency coefficient ($Pa \cdot s^n$), $\dot{\gamma}$ is the shear rate (s^{-1}), and n is the flow behavior index (dimensionless).

2.13. Texture profile analysis (TPA)

The textural properties of the fresh gel beads were evaluated using a TA.XTC-20 texture analyzer (Shanghai Baosheng Industrial Development Co., Ltd., China), fitted with a TA/0.5 gel probe. The analysis was carried out following the method of Wan et al. (2021), with some modifications. The pre-test, testing, and post-test speeds were all set at 1.0 mm/s, and the compression strain was adjusted to achieve 50% deformation of the gel beads. A trigger force of 5.0 g was applied, with a holding time of 5 s between compressions.

2.14. In vitro prebiotic activity evaluation

The effect of five different dried gel bead formulations on the proliferation of *Lactiplantibacillus plantarum* Lp3a was evaluated following the method of Lee et al. (2023), with slight modifications. Briefly, *Lactiplantibacillus plantarum* Lp3a powder was activated in MRS broth at 37°C for 48 h before use. Subsequently, 200 μL of the activated bacterial culture was inoculated into 10 mL of carbon-free MRS broth supplemented with 1% (*w/v*) of each gel bead sample. Carbon-free MRS broth without any added samples served as the control group. After incubation at 37°C for 48 h, the bacterial suspension was serially diluted from 10^{-1} to 10^{-8} and spread onto MRS agar plates. Following an additional 48-h incubation at 37°C, the number of colony-forming units (CFU) was counted and expressed as CFU/mL using Eq. (6):

$$CFU/mL = \frac{Number\ of\ colonies \times Dilution\ factor}{Volume\ of\ inoculum\ (mL)} \quad (6)$$

2.15. Statistical analysis

Experimental data were expressed as the mean ± standard deviation. Statistical analysis was performed using one-way analysis of variance (ANOVA) with SPSS 25 software, with $P<0.05$ indicating a significant difference. All experimental groups were performed in triplicate.

3. Results and analysis

3.1. Visual appearance

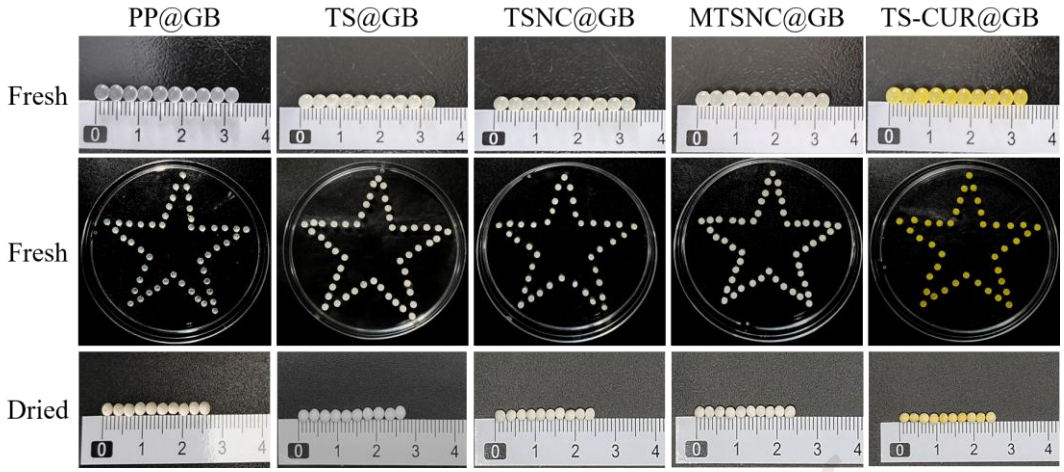

Fig. 1. Visual appearance of PP@GB, TS@GB, TSNC@GB, MTSNC@GB, and TS-CUR@GB gel beads.

The visual appearance of the fresh and dried PP@GB, TS@GB, TSNC@GB, MTSNC@GB, and TS-CUR@GB gel beads was illustrated in **Fig. 1**. All five types of fresh gel beads displayed a regular spherical shape, uniform size distribution, and smooth surface, with diameters ranging from approximately 3.3 to 3.4 mm. PP@GB appeared transparent, whereas the gel beads containing starch-based formulations (TS@GB, TSNC@GB, and MTSNC@GB) exhibited a milky-white appearance. Notably, the gel bead incorporating the starch-curcumin complex (TS-CUR@GB) displayed a distinct yellow coloration due to the intrinsic hue of curcumin. Previous studies have suggested that the average particle size suitable for direct swallowing by adults ranges from 2 to 4 mm (Jiang et al., 2024). Therefore, the gel beads developed in this study possess suitable dimensions for use as easily ingestible carriers in food or pharmaceutical applications. Additionally, a reduction in bead diameter was observed after freeze-drying compared to the fresh state. This shrinkage is likely due to water loss during the freeze-drying process, resulting in structural contraction and a decrease in overall volume (Lee et al., 2023).

3.2. FTIR analysis

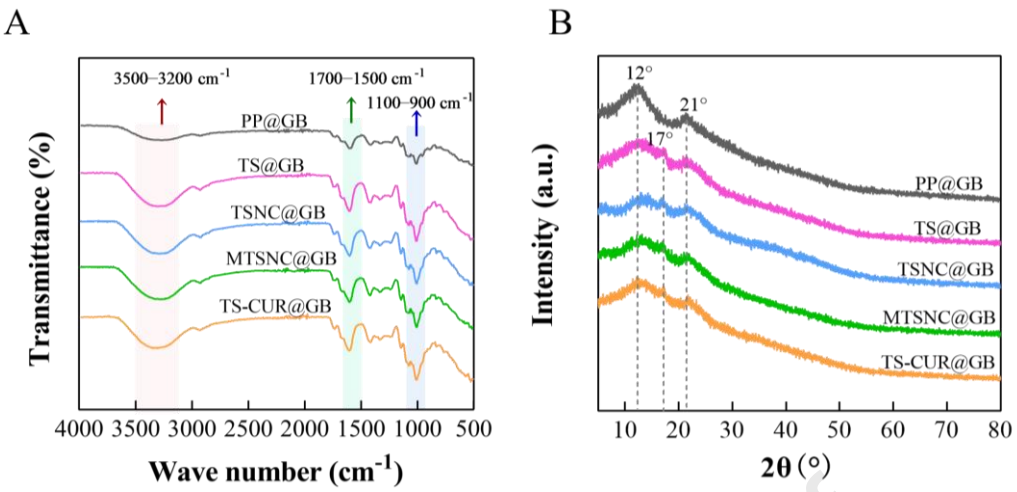

Fig. 2. FTIR spectra (A) and XRD patterns (B) of PP@GB, TS@GB, TSNC@GB, MTSNC@GB, and TS-CUR@GB gel beads.

The chemical bonds and functional groups present in PP@GB, TS@GB, TSNC@GB, MTSNC@GB, and TS-CUR@GB were analyzed using FTIR to investigate potential molecular interactions among the constituent components, as shown in **Fig. 2A**. PP@GB exhibited a broad absorption peak in the range of 3500−3200 cm^{-1}, which corresponds to the stretching vibration of the O−H group, indicating the presence of hydrogen-bonded hydroxyl functionalities. A peak between 2900−2800 cm^{-1} was attributed to the stretching vibrations of the −CH group. The wide peak in the region of 1700−1500 cm^{-1} was associated with the asymmetric and symmetric stretching vibrations of the COO− groups (Yang et al., 2024; Vaziri et al., 2018). Additionally, the absorption peaks observed between 1100−900 cm^{-1} corresponded to the C−O and C−C stretching vibrations associated with glycosidic linkages and pyran ring structures. These characteristic FTIR absorption features are consistent with those previously reported for pectin-based gel beads by Sarkar et al. (2024) and Günter et al. (2022).

The FTIR spectra of TS@GB, TSNC@GB, MTSNC@GB, and TS-CUR@GB were similar to that of PP@GB, with no new absorption peaks observed upon the incorporation of different starch matrices, indicating that no new chemical bonds were formed during the formation of the composite gel systems. However, an increase in the intensity of the O−H stretching vibration band in the 3500−3200 cm^{-1} region was observed in the starch-containing gel beads, indicating enhanced hydrogen bonding

interactions between pectin and starch molecules, which is due to the increased availability of hydroxyl groups in starch derivatives, forming additional hydrogen bonds with the pectin main chain. This extended hydrogen bond network promotes the formation of a more cohesive and rigid three-dimensional structure (Li et al., 2024). A similar enhancement in hydrogen bonding within polysaccharide-starch composite gels has been reported by Ren, Jiang, et al. (2024). Moreover, the increased intensity of the absorption band in the 1700−1500 cm^{-1} range further supports the presence of stronger intermolecular hydrogen bonding between starch and pectin (Lenie et al., 2024). The intensification of the spectral features in the 1100−900 cm^{-1} range was assigned to C−O−C glycosidic bond vibrations in glucose units, which was interpreted as evidence of enhanced hydrogen bonding between hydroxyl groups and different glucose units within the matrix (Han et al., 2023). These FTIR spectral changes provide direct molecular-level evidence for the strengthening of hydrogen bonds in the composite gel. Crucially, these enhancements are consistent with the improvement of macroscopic properties: the enhanced hydrogen bond network directly corresponds to the denser microstructure observed by SEM images (**Fig. 4**), the decrease in swelling rate determined by swelling experiment (**Fig. 5B**), and the increase in mechanical strength measured by texture analysis (**Fig. 7**). These multi-scale results collectively demonstrated that enhanced hydrogen bonds play a crucial role in improving the structural integrity and functional performance of composite gel beads.

3.3. XRD analysis

The crystal properties of PP@GB, TS@GB, TSNC@GB, MTSNC@GB, and TS-CUR@GB gel beads were characterized using XRD, as shown in **Fig. 2B**. PP@GB exhibited two broad diffraction peaks at approximately 2θ = 12° and 21°, which are characteristic of semi-crystalline materials (Liu et al., 2024). Upon incorporating various starch-derived materials, the intensity of these diffraction peaks was reduced in TS@GB, TSNC@GB, MTSNC@GB, and TS-CUR@GB, indicating the partial loss of crystal order and the transition to amorphous structure in the composite system. This phenomenon is commonly observed in polymer composite systems, where water absorption during blend preparation, along with inter- and intramolecular hydrogen

bonds between polymers, leads to the loss of crystal structure (Lopes et al., 2023). The decrease in crystallinity is particularly significant as it often correlates with enhanced functional properties, such as improved encapsulation efficiency and faster dissolution rate of the water-insoluble bioactive due to the free volume in amorphous regions and an increase in the lattice free energy. Consequently, low-crystallinity formulations are expected to exhibit higher bioavailability compared to higher-crystallinity formulations (Ubeyitogullari et al., 2019).

Additionally, a new, weak diffraction peak appeared at $2\theta = 17°$ in the composite gel beads, which may correspond to the characteristic crystalline reflection of the incorporated starch-based materials. As previously reported, turmeric starch and its derivatives exhibited distinct diffraction peaks at $2\theta = 17°$ (Zhu et al., 2025). Therefore, the emergence of this peak in the composite systems confirmed the successful incorporation of starch-derived materials into the pectin matrix. However, the low intensity of this peak in our composites, compared to the sharp peak of native starch, indicated that the starch crystals underwent partial destruction during the composite formation process. This finding is consistent with those of Ren, Jiang, et al. (2020), who demonstrated that gelatinization and complexation can lead to a transformation from a crystalline to an amorphous structure in starch-polysaccharide complexes, as evidenced by a decrease in the intensity of the characteristic peak. Therefore, the XRD results demonstrated the successful formation of an amorphous-crystalline composite system where the starch components are integrated into the pectin network, leading to a material with an improved crystalline architecture that is anticipated to be more amenable to bioactive compound encapsulation.

3.4. TGA analysis

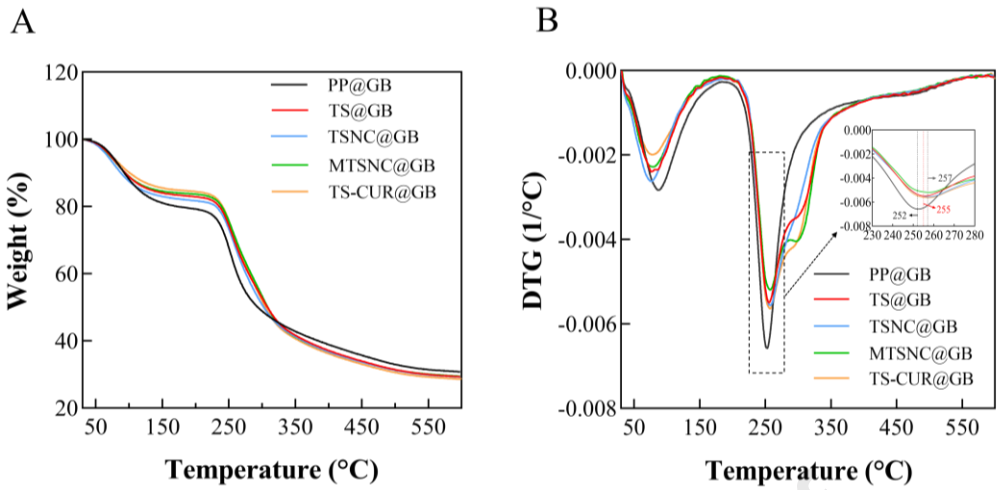

Fig. 3. TGA curves (A) and DTG curves (B) of PP@GB, TS@GB, TSNC@GB, MTSNC@GB, and TS-CUR@GB gel beads.

The thermal stability of PP@GB, TS@GB, TSNC@GB, MTSNC@GB, and TS-CUR@GB gel beads was assessed using TGA, as shown in **Fig. 3**. The TGA curves of all samples exhibited three distinct stages of thermal degradation (**Fig. 3A**). The first stage occurred between 30°C and 120°C, primarily due to the evaporation of bound water within the gel matrix as the temperature increased (Xiao et al., 2022). The second stage centered around 250°C, during which all gel beads showed significant mass loss. This weight loss might be due to the dehydration of sugar rings, decomposition of pectin and starch structures, and volatilization of other organic components (Singh et al., 2017). Notably, PP@GB exhibited a maximum weight loss of approximately 34% during this stage, whereas the composite gel beads showed lower losses of around 29%. Furthermore, the peak degradation temperature for PP@GB was approximately 252°C, while the composite formulations exhibited a shift to higher degradation temperatures (**Fig. 3B**), indicating that the incorporation of starch-based materials enhanced the thermal resistance of the gel network, thereby improving overall thermal stability. This enhancement can be attributed to stronger intermolecular interactions among pectin, starch molecules, and Ca^{2+}, which increase cross-linking density and structural integrity within the composite network, thus resisting chain scission during heating and reducing thermal degradation (Raza et al., 2024). The third stage of degradation, occurring between 300°C and 600°C, reflects the complete breakdown of residual organic matter and the eventual formation of inorganic ash residues (Ubeyitogullari et al., 2016).

Combined with FTIR analysis, it is likely that starch-based derivatives promoted the formation of a more stable three-dimensional gel network by enhancing intermolecular interactions, ultimately improving thermal stability. These results can provide important references for designing hydrogel systems with excellent thermal stability and mechanical properties.

3.5. SEM analysis

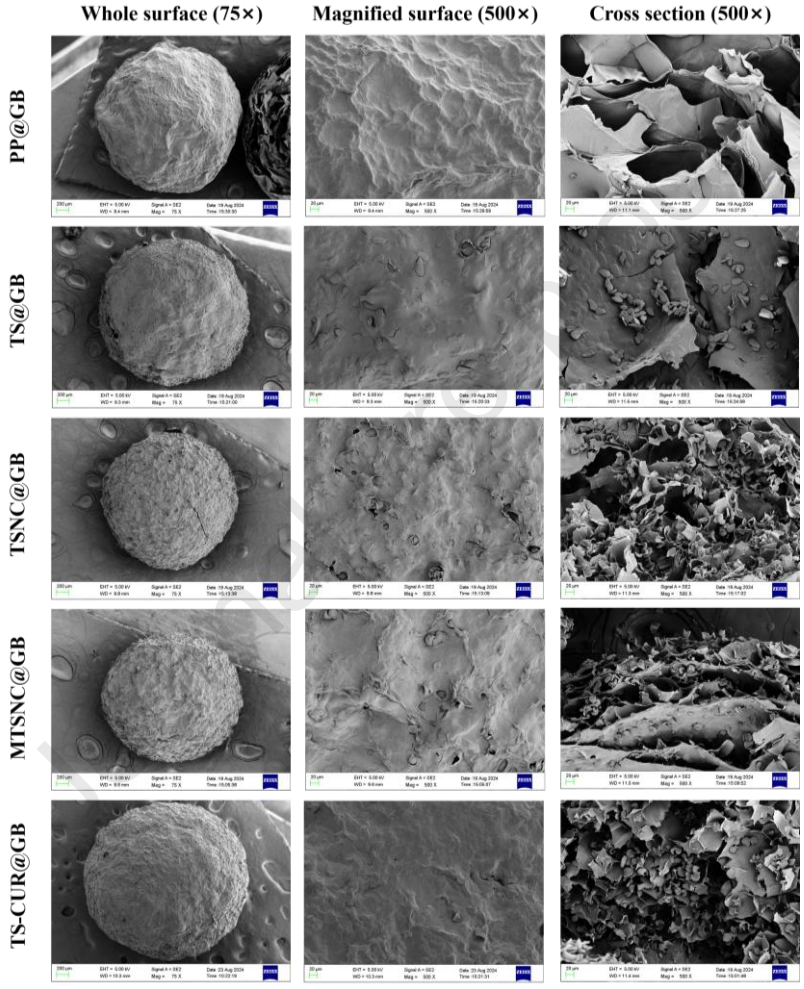

Fig. 4. SEM images of PP@GB, TS@GB, TSNC@GB, MTSNC@GB, and TS-CUR@GB gel beads.

The surface morphology and internal cross-sectional structure of dried PP@GB, TS@GB, TSNC@GB, MTSNC@GB, and TS-CUR@GB gel beads were observed using SEM, as shown in **Fig. 4**. At a lower magnification of 75×, all five gel beads exhibited a generally spherical morphology, confirming the successful formation of structurally intact beads through Ca^{2+}-mediated cross-linking of the pectin-starch matrix. However, their surfaces appeared rough, rugged, and partially shrunken, which

may be attributed to structural collapse caused by moisture loss during freeze-drying (Bušić et al., 2018). At a higher magnification of 500×, a distinct "vein"-like network structure was observed on the surface of PP@GB, which is characteristic of ionically cross-linked hydrogels formed between Ca^{2+} and carboxylate groups in polysaccharide chains (Qi et al., 2020). Subsequently, the incorporation of various starch-derived materials into the pectin matrix led to significant structural changes in the gel beads. As reported in our previous study, turmeric starch exhibited a flat oval shape, while starch nanoparticles and complexes displayed a helical morphology (Zhu et al., 2025). Upon integration into the pectin-based gel matrix, these starch components altered the bead surface, resulting in a progressive reduction in surface wrinkles and protrusions. Moreover, distinct morphological features corresponding to the respective starch matrices were observed on the surfaces of the composite gel beads, indicating successful embedding and uniform dispersion of starch-derived materials within the pectin network.

Additionally, the internal cross-sectional structure of the gel beads was also observed. All five formulations exhibited a laminar structure with irregular cavities, which may be attributed to structural shrinkage and deformation during the freeze-drying process (Li et al., 2021). Notably, PP@GB displayed relatively larger pores and cavities, whereas the starch-containing composite gel beads exhibited a more uniform honeycomb-like porous structure with smaller and densely packed pores. This tightly interconnected microstructure suggests enhanced cross-linking among starch, pectin, and Ca^{2+}, highlighting the role of starch-based fillers as structural modifiers that promote the formation of a robust and compact gel network (Raza et al., 2024; Cortés-Camargo et al., 2023). Dumitriu et al. (2011) previously demonstrated that increased cross-linking density correlates with reduced pore size, resulting in a denser and more mechanically stable hydrogel structure. Similarly, Lozano-Vazquez et al. (2015) reported that the incorporation of modified tapioca starch into sodium alginate-based gel beads acted as a reinforcing filler, enhancing structural integrity and promoting the formation of a well-defined porous network. The presence of a well-developed porous structure is also relevant to the hydration behavior of the gel systems. Porosity and

internal cavities have been associated with improved water penetration and retention capacity within the matrix, thereby contributing to enhanced water-holding properties (Paswan et al., 2024). These observations are consistent with the WHC and LF-NMR results, which collectively indicate that the composite gel bead formulations exhibit superior water retention capabilities compared to the pure pectin-based system.

3.6. Water holding capacity (WHC)

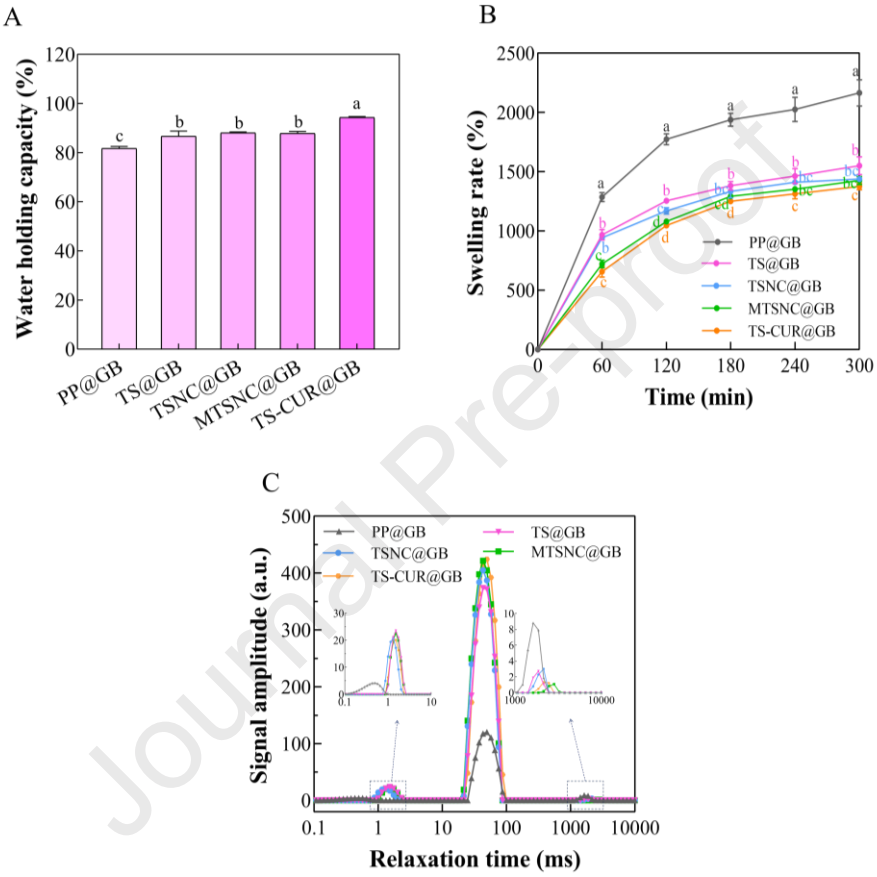

Fig. 5. Water holding capacity (A), swelling behavior (B), and water distribution profiles (C) of PP@GB, TS@GB, TSNC@GB, MTSNC@GB, and TS-CUR@GB gel beads. Different lowercase letters indicate significant differences (P<0.05).

Water holding capacity (WHC) is a key functional property of hydrogel systems, reflecting the ability of the three-dimensional polymeric network to retain water. The WHC values of the five gel bead formulations were presented in **Fig. 5A**. As shown, the WHC of PP@GB was approximately 80%, while the WHC of TS@GB, TSNC@GB, and TS-CUR@GB increased to around 85% (P<0.05). This improvement may be attributed to the enhanced ionic interactions between calcium ions and the carboxyl groups of pectin or hydroxyl groups of starch, which facilitate the formation of a more

compact hydrogel network capable of effectively entrapping water molecules (Bu et al., 2022). Both the swelling rate (**Fig. 5B**) and texture analysis (**Fig. 7**) results can support this trend. The reduced swelling rate, enhanced hardness and springiness of the composite gel beads jointly indicate a denser, more cross-linked, and less porous network structure, which effectively inhibits water diffusion and improves water-holding capacity. In addition, similar findings have also been reported by Ren, Jiang, et al. (2020) in polysaccharide-starch complex systems, who demonstrated that the interaction between polysaccharides and starch granules can lead to greater repulsion and retain more water molecules in the gel matrix, further supporting our conclusion. Notably, the WHC of TS-CUR@GB reached 90.84% (P<0.05), representing an increase of approximately 13.6% compared to PP@GB, suggesting that the incorporation of the starch-curcumin complex further enhanced the water-holding capacity of the gel beads. This enhancement may be attributed to the phenolic hydroxyl groups of curcumin forming strong hydrogen bonds with both starch and pectin molecules, leading to a more densely cross-linked and ordered microstructure that entangles more water within the gel matrix (Wang et al., 2018). This high WHC is crucial for the application of these beads as delivery carriers, as the retained water molecules help to stabilize the interactions among the system components and maintain the structural integrity of the bead throughout the delivery process, thereby protecting the encapsulated bioactive compound (Li et al., 2024).

3.7. Swelling rate

The swelling behaviors of PP@GB, TS@GB, TSNC@GB, MTSNC@GB, and TS-CUR@GB in deionized water were measured and presented in **Fig. 5B**. All five gel beads exhibited similar swelling profiles, with a rapid increase in swelling rate during the initial 60 min, followed by a gradual deceleration as equilibrium was approached. This initial rapid uptake can be attributed to the immediate hydration of hydrophilic functional groups present in both pectin and starch molecules, as well as the presence of porous structures formed during the freeze-drying process, which facilitate efficient water penetration and retention (Yang et al., 2024). A comparable swelling profile has been observed in alginate-based gel beads by Li et al. (2021), who reported that the

swelling rates of all samples gradually increased within 6 h, reaching the highest swelling rate after 6 h.

Among all formulations, PP@GB exhibited the highest swelling rate, which may be attributed to its relatively loose gel structure and larger pores, as observed in the SEM analysis (**Fig. 4**), facilitating enhanced water penetration and retention (Hu et al., 2021). In contrast, the incorporation of various starch-based matrices resulted in a significant decrease in the swelling rates of TS@GB, TSNC@GB, MTSNC@GB, and TS-CUR@GB compared to PP@GB (P<0.05). This reduction is likely due to enhanced cross-linking interactions among starch, pectin, and calcium ions, which promote stronger intermolecular bonding and the formation of a more compact and ordered gel network, thereby limiting water diffusion and reducing the overall swelling capacity (Hu et al., 2021). A similar trend was reported by Chen et al. (2024), who found that incorporating starch and protocatechuic acid into the shell layer of alginate-based gel beads significantly reduced their swelling behavior. Notably, the mean swelling rate of TS-CUR@GB was slightly lower than that of the other composite groups, although the differences were not all statistically significant. This trend indicates that the presence of curcumin may partially weaken the repulsive force between carboxyl groups, thereby reducing the expansion of hydrogel beads and resulting in a lower swelling phenomenon (Chen et al., 2024; Wang et al., 2021). This reduced swelling behavior is consistent with the SEM observation, gel beads with a lower swelling rate exhibited denser and more uniform pore morphology (**Fig. 4**), thus restricting the penetration of water molecules. Meanwhile, the increasing trend in mechanical hardness (**Fig. 7A**) also provided supportive observations for a more robust network structure and a higher degree of cross-linking, although this difference did not reach statistical significance. These findings are consistent with previous results that gel beads with lower swelling rates typically exhibit denser microstructures, which can enhance mechanical stability and shape retention (Su et al., 2023). In summary, our findings demonstrated that the integration of starch and bioactive compounds can effectively modulate the microstructure and swelling properties of pectin gel beads, offering promising potential for controlled release applications in both food and biomedical fields.

3.8. Low-field nuclear magnetic resonance (LF-NMR) analysis

Water distribution within hydrogel matrices plays a critical role in determining their structural properties, stability, and functional performance. To investigate the water distribution within the gel networks, LF-NMR was employed, with the transverse relaxation time (T_2) serving as a highly sensitive indicator of water molecule dynamics and a key parameter reflecting the physical state of water (Ren, Rong, et al., 2020). The water migration behavior of PP@GB, TS@GB, TSNC@GB, MTSNC@GB, and TS-CUR@GB was analyzed using T_2 relaxation measurements obtained by LF-NMR, as shown in **Fig. 5C**. The NMR relaxation curves of all samples exhibited three distinct peaks within the relaxation time range of 0.1–10000 ms, corresponding to three different states of water. Specifically, T_{21} (1–10 ms) corresponds to bound water tightly associated with the polymer matrix, T_{22} (10–100 ms) represents immobilized or fixed water trapped within the gel network, and T_{23} (>100 ms) reflects free water with high mobility (Wang et al., 2024). Moreover, the peak area under each relaxation component reflects the relative proportion of the corresponding water state.

Among all samples, the T_{22} peak was the most prominent, indicating that immobilized water constituted the dominant fraction within the gel matrix, followed by bound water, while free water accounted for the smallest proportion. Notably, PP@GB exhibited the lowest proportion of immobilized water and a relatively higher content of free water, which is consistent with its relatively porous and loosely structured network, resulting in greater water mobility and reduced water retention capacity. In contrast, the starch-containing gel beads showed a shift toward more tightly bound water, indicating stronger interactions between water molecules and the polymer network due to enhanced cross-linking and hydrogen bonding within the gel network, which restricted water mobility and reduced the amount of diffusible free water (Jiang et al., 2022). This observation was further supported by the reduced T_{23} peak area observed in the composite gel beads, indicating a lower content of free water. Moreover, these findings are consistent with the WHC analysis results shown in **Fig. 5A**, further demonstrating that the composite gel system maintains a high water-holding capacity due to the restricted movement of water molecules within the gel matrix. The consistency between

T_2 relaxation behavior and WHC measurements highlights the role of starch in modifying the hydrogel's architecture, thereby improving its capacity to entrap and stabilize water. These findings are supported by previous reports on polysaccharide-starch composite systems (Jiang et al., 2024; Ye et al., 2018).

3.9. Rheological properties analysis

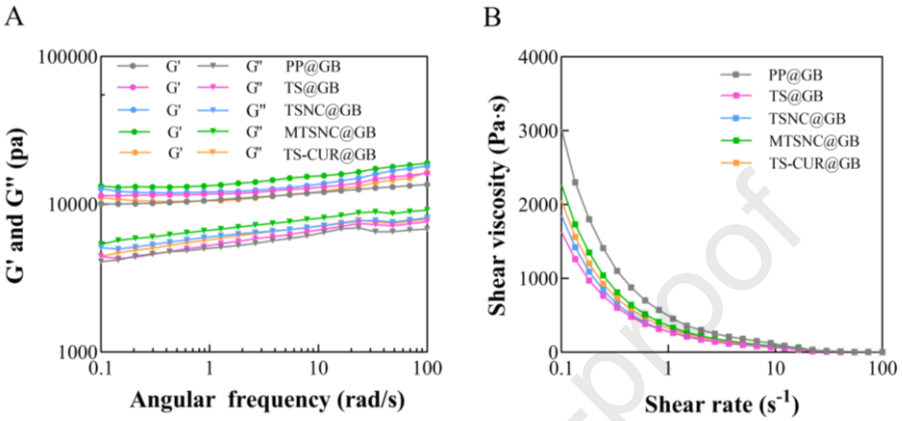

Fig. 6. Dynamic modulus variation curves (A) and shear viscosity variation curves (B) of PP@GB, TS@GB, TSNC@GB, MTSNC@GB, and TS-CUR@GB gel beads.

Dynamic rheological properties provide critical insights into the viscoelastic behavior of materials under mechanical stress, offering valuable guidance for process optimization and quality control in food and pharmaceutical applications (Qiu et al., 2024). In dynamic oscillatory testing, the storage modulus (G′) reflects the elastic behavior of a material, whereas the loss modulus (G″) represents its viscous characteristics. The variation of G′ and G″ with angular frequency for PP@GB, TS@GB, TSNC@GB, MTSNC@GB, and TS-CUR@GB was presented in **Fig. 6A**. Across the entire angular frequency range, G′ remained consistently higher than G″ for all samples, indicating that the gel beads exhibited predominantly elastic behavior and displayed typical characteristics of gels (Xiao et al., 2022). Among all samples, PP@GB exhibited the lowest G′ and G″ values, suggesting a relatively weak gel network. This can be attributed to the pure pectin system, which relies solely on calcium ion-mediated cross-linking of pectin molecules, resulting in a less dense and structurally weaker network (Almeida et al., 2021). However, the incorporation of various starch-based fillers significantly enhanced both G′ and G″ to varying extents, reflecting improved structural rigidity and viscoelastic performance. This improvement can be attributed to

stronger cross-linking among starch, pectin, and calcium ions, which contribute to a more compact and ordered gel matrix. A similar trend was observed by Li et al. (2024), who demonstrated that the addition of sodium alginate to a pectin-based gel increased the network density and consequently enhanced both G′ and G″. Notably, the G′ and G″ values of TS@GB, TSNC@GB, and MTSNC@GB increased progressively compared to PP@GB, as presented in **Table S1** in the supplementary materials. This sequential enhancement may be attributed to that as starch filler evolved from its natural form, to the nanoparticle state, and then to the modified nanoparticle form, the binding sites and intermolecular among starch fillers, pectin molecules, and calcium ions increased successively, promoting the formation of calcium ion-mediated ionic crosslinking and leading to a more ordered and densely cross-linked gel structure (Wang et al., 2018). Interestingly, TS-CUR@GB exhibited lower G′ and G″ values than MTSNC@GB, suggesting that the incorporation of curcumin reduced the dynamic modulus. We speculated that the reason might be that the incorporation of curcumin interfered with the original cross-linking process of starch, pectin matrix, and calcium ions, reducing the fluidity of polymer chain segments, thereby resulting in a decline in the overall viscoelastic response ability of the material under minor deformation, manifested as a decrease in modulus. This inference is consistent with the conclusion reported by Xiao et al. (2023) that curcumin may affect the binding of starch to other matrix components through molecular competitive interactions, hinder the cross-linking and entanglement of starch molecular chains, reduce the number of effective junction regions within the gel network, and ultimately diminish the viscoelastic strength of the system. The power-law model fitting parameters for the frequency dependence of G′ and G″ further corroborated these observations (**Table S2)**. The flow behavior indices (n′ and n″) and the ratio k″/k′ for all samples were substantially less than 1, collectively confirming typical “solid-like” gel behavior (Zhang et al., 2021). Within this framework, PP@GB exhibited the lowest stiffness coefficients (k′ = 10.80 kPa·s^n, k″ = 5.08 kPa·s^n), consistent with a sparse Ca^{2+}-pectin network. The incorporation of starch fillers led to a stepwise increase in both k′ and k″ (P<0.05), indicating enhanced cross-linking density and the formation of a more rigid gel structure.

Shear viscosity is defined as the resistance of a fluid to flow under applied shear stress. The steady-state shear viscosity profiles of PP@GB, TS@GB, TSNC@GB, MTSNC@GB, and TS-CUR@GB are shown in **Fig. 6B**. All samples exhibited a progressive decrease in viscosity with increasing shear rate, demonstrating shear-thinning behavior characteristic of pseudoplastic fluids (Ren, Jiang, et al., 2020). This behavior can be attributed to the disruption of the internal gel network under shear forces, resulting in the transition of molecules from a structured network to a more fluid-like state, thereby reducing the apparent viscosity (Li et al., 2024). Similar rheological behavior has been reported in other starch-based and hydrogel systems (Chen et al., 2014). Among all samples, PP@GB exhibited the highest shear viscosity, indicating that greater shear stress is required to disrupt the pectin gel matrix. This may be due to the high intrinsic viscosity of pectin, which results in extensive chain entanglements that confer strong resistance to deformation (Jiang et al., 2015). In contrast, the shear viscosities of all starchy gel beads (TS@GB, TSNC@GB, MTSNC@GB, and TS-CUR@GB) were lower than that of PP@GB (**Table S3**), indicating that the starch fillers, as the "diluent phase" incorporated into the pectin network, had a dominant weakening effect on the overall viscosity, manifested as a decrease in viscosity. It was further observed that the viscosities of TS@GB, TSNC@GB, and MTSNC@GB showed a gradually increasing trend. This may be due to as the starch filler evolved from its natural form to nanoparticles and then to modified nanoparticles, the interaction among starch, pectin, and calcium ions gradually strengthened, and the structural integrity of the gel network gradually improved, thereby enhancing the shear resistance. Notably, TS-CUR@GB exhibited lower shear viscosity than MTSNC@GB, indicating that the incorporation of curcumin further weakened the shear resistance of the gel network. Such interactions may reduce physical entanglement nodes among starch molecular chains, leading to a less organized structure and reduced resistance to shear stress (Wang et al., 2018). The parameters obtained through power-law model fitting further revealed the mechanism of the above changes (**Table S4**). The correlation coefficients (R^2) of all samples were greater than 0.99, indicating that the power law equation can be used to fit the steady-state shear

curve. The flow behavior index (n) reflects a fluid's deviation from Newtonian behavior, where n=1 indicates a Newtonian fluid and n<1 characterizes a pseudoplastic (shear-thinning) fluid. The obtained n values of all formulations were less than 1, further verifying the shear-thinning characteristics of these systems (Lin et al., 2021). The variation of the consistency coefficient K value reflects the strength of the network structure. The K value of PP@GB was the highest (474.60 $Pa \cdot s^n$), confirming the stronger chain entanglement and flow resistance in the pure pectin network. However, after the addition of starch derivatives, the K values of the composite gel beads decreased significantly to varying degrees (P<0.05), demonstrating that the introduction of starch fillers weakened the network continuity.

In conclusion, rheological analysis revealed that the composite gel beads possess both excellent mechanical strength (high dynamic modulus) and superior processing fluidity (low shear viscosity), which provides an ideal material basis for the controllable processing and targeted delivery of functional gel products.

3.10. Textural properties

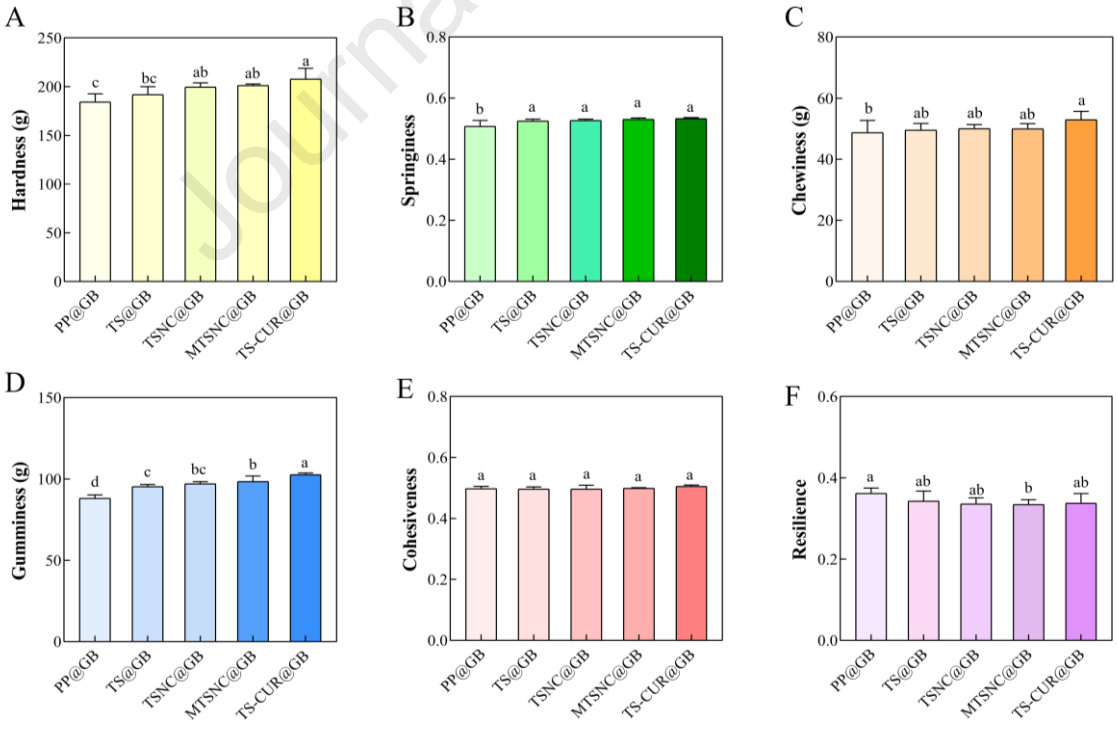

Fig. 7. Texture properties of PP@GB, TS@GB, TSNC@GB, MTSNC@GB, and TS-CUR@GB gel beads. Different lowercase letters indicate significant differences (P<0.05).

Texture analysis offers valuable insight into the mechanical and structural characteristics of gel systems. The texture properties, including hardness, springiness, chewiness, gumminess, cohesiveness, and resilience, of PP@GB, TS@GB, TSNC@GB, MTSNC@GB, and TS-CUR@GB were evaluated and shown in **Fig. 7**. Compared to PP@GB, the hardness of TS@GB, TSNC@GB, MTSNC@GB, and TS-CUR@GB increased by 4.16%, 8.40% (P<0.05), 9.23% (P<0.05), and 12.75% (P<0.05), respectively. This enhancement can be attributed to the formation of hydrogen bonds between the hydroxyl groups of starch and pectin molecules, which strengthen the gel network and enhance the mechanical integrity of the beads (Bu et al., 2023). Notably, TS-CUR@GB exhibited the highest hardness, which may be attributed to the incorporation of curcumin that establishes strong hydrogen bonding interactions with both starch and pectin molecules, thereby reinforcing the structural integrity and stability of the gel matrix (Wang et al., 2018).

Similar trends were observed for springiness, chewiness, and gumminess. Compared to PP@GB, the enhanced interactions between starch and pectin in the composite gel beads contribute to a denser gel network, which increases water-holding capacity and helps maintain the softness and extensibility of the gel beads, thereby enhancing their springiness (Wang et al., 2018). The simultaneous increase in hardness and springiness indicates an enhanced gel network structure. This network possesses higher mechanical strength and greater elasticity, requiring more energy for deformation, which is consistent with the increased chewiness and gumminess. In contrast, the resilience of TS@GB, TSNC@GB, MTSNC@GB, and TS-CUR@GB exhibited a decreasing trend compared to PP@GB. This reduction may be due to the interference of starch-based fillers with the alignment and cross-linking of pectin chains, potentially hindering the molecular rearrangements required for structural recovery after deformation. Consequently, the ability of the gel beads to recover their original shape upon removal of mechanical stress was diminished (Wang et al., 2021).

Overall, the texture properties are consistent with the microstructure morphology (**Fig. 4**) and swelling properties (**Fig. 5B**), jointly indicating that the addition of starch derivatives and curcumin enhances the mechanical strength and water retention of

pectin gels, which provides a comprehensive material basis for designing functional gels with customized performance, suitable for food and pharmaceutical applications.

3.11. In vitro prebiotic activity evaluation

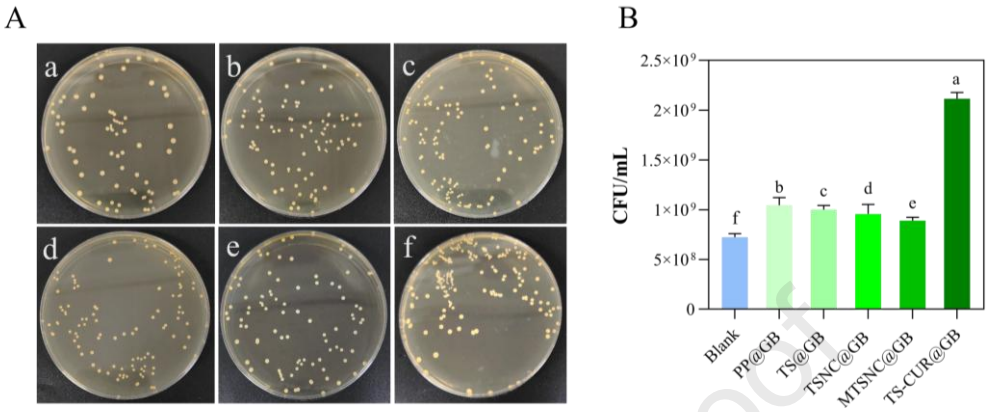

Fig. 8. Colonization of *Lactiplantibacillus plantarum* Lp3a at a concentration of 10^{-6} after different sample treatments (A): Blank (a), PP@GB (b), TS@GB (c), TSNC@GB (d), MTSNC@GB (e), and TS-CUR@GB (f). Effect of different samples on the proliferation of *Lactiplantibacillus plantarum* Lp3a (B). Different lowercase letters indicate significant differences (P<0.05).

Lactiplantibacillus plantarum is a common and representative probiotic strain that has been demonstrated to stimulate the growth of intestinal microbiota, inhibit the proliferation of harmful microorganisms, and reduce the incidence of gastrointestinal diseases, thereby conferring multiple health benefits (Razavi et al., 2021). Previous studies have shown that pectin can be fermented by colonic microbiota and exerts prebiotic effects, promoting the growth of beneficial bacteria (Zhang et al., 2025). Therefore, in this study, *Lactiplantibacillus plantarum* Lp3a was selected as the representative model strain to systematically evaluate the prebiotic potential of the five gel bead formulations.

As shown in **Fig. 8B**, in the carbon-source-free medium, the colony count in the control group was 7.23×10^8 CFU/mL, while the colony counts of PP@GB, TS@GB, TSNC@GB, MTSNC@GB, and TS-CUR@GB groups significantly increased to 1.05×10^9, 1.00×10^9, 9.57×10^8, 8.90×10^8, and 2.12×10^9 CFU/mL (P<0.05), respectively. These results indicated that all five gel beads exhibited prebiotic activity by positively influencing the growth of *Lactiplantibacillus plantarum* Lp3a. Notably, the colony

counts in the PP@GB, TS@GB, TSNC@GB, and MTSNC@GB groups followed a gradually decreasing trend. This may be attributed to the relatively low crosslinking degree in the pure pectin gel beads (PP@GB), which allows for easier water absorption, swelling, and even structural disintegration, thereby facilitating the decomposition and utilization of the gel matrix by microorganisms and resulting in higher colony counts. In contrast, the cross-linking density increases progressively in TS@GB, TSNC@GB, and MTSNC@GB, leading to more compact structures, restricting water penetration and swelling capacity, thereby reducing the accessibility of microbial to the prebiotic components and consequently weakening the stimulatory effect on the growth of *Lactiplantibacillus plantarum* Lp3a.

Interestingly, the TS-CUR@GB group exhibited a significantly higher colony count, reaching 2.92 times that of the control group ($P<0.05$). Previous studies have indicated that curcuminoids possess prebiotic activity and can promote the proliferation of beneficial gut bacteria while modulating the composition of the intestinal microbiota (Bhola et al., 2024). Therefore, the significant increase in probiotic counts in the TS-CUR@GB group may be attributed to two potential mechanisms. On the one hand, curcumin itself may directly regulate gut microbiota and stimulate the growth of *Lactiplantibacillus plantarum* Lp3a. On the other hand, the strong interaction between curcumin and pectin molecules may generate a synergistic effect, potentially enhance the bioavailability or metabolic accessibility of the prebiotic substrate, and further promote microbial growth (Li et al., 2022). In summary, integrating curcumin into a pectin-based delivery system not only helps preserve its original bioactive properties but also enhances its proliferation-promoting effect on representative probiotic strains. More importantly, this dual functionality highlights the potential of the prebiotic activity of such composite systems, providing an effective material basis and strategic direction for the development of new formulations with enhanced prebiotic functions.

4. Conclusions

In this study, pectin/starch composite gel beads were successfully prepared using a simple ionic gelation method, and their structural characteristics, physicochemical properties, and functional performance were systematically investigated. The results

indicated that all five gel beads exhibited well-defined spherical morphologies with diameters ranging from 3.3 to 3.4 mm. Microstructural analysis revealed that the internal structure of the gel beads was composed of irregular cavities and a layered morphology, and the incorporation of starch derivatives enhanced structural compactness, resulting in a denser and uniformly distributed porous architecture. FTIR and XRD analysis confirmed increased intermolecular interactions and reduced crystallinity upon starch integration. TGA results indicated enhanced thermal stability in the starch-containing gel systems. WHC and LF-NMR analysis demonstrated that the addition of starch matrix significantly improved moisture retention by 6.06%–15.44%, while reducing the swelling rate by 26.16%–37.02%. Texture profile and rheological testing further revealed significant improvements in hardness (4.16%–12.75%), springiness (3.40%–4.96%), chewiness (1.71%–8.63%), and gumminess (8.09%–16.51%), along with enhanced viscoelastic behavior. Furthermore, all five gel bead formulations exhibited favorable prebiotic activity, significantly promoting the growth of *Lactiplantibacillus plantarum* Lp3a. Notably, the TS-CUR@GB formulation, which incorporated curcumin, demonstrated a synergistic enhancement in probiotic proliferation. Overall, starch-based derivatives with gradient-enhanced structure and function exhibited a gradually enhancing regulatory effect on the structural properties of pectin gel beads, especially those enriched with the bioactive component curcumin, demonstrating a dual enhancement in both structural characteristics and functional performance. These findings provide a comprehensive understanding of the mechanism by which starch-based fillers modulate pectin gelation and offer valuable insights into the design and development of novel functional gel bead formulations with enhanced performance.

However, this study has certain limitations that should be acknowledged. Although the current findings initially confirmed that these gel beads have a growth-promoting effect on a specific model strain, experiments on a single strain are not sufficient to fully reflect their actual role in the complex intestinal flora. In subsequent studies, more strains should be introduced to systematically evaluate the effects of gel beads on the proliferation of multiple probiotics, thereby comprehensively assessing their prebiotic

efficacy. In addition, this gel bead system can be further applied in real food environments (such as yogurt or beverage systems) to evaluate its impact on the physicochemical properties and sensory attributes of products, thereby providing a theoretical basis and technical foundation for practical food applications.

Acknowledgement

This work was supported by the Key Technology Research and Development Program of Shandong Province, China (2024TZXD007).

References

Almeida, S. F., Silva, G. K. C., Toledo, M. N. A., & Sato, A. C. K. (2021). Modulating porosity and mechanical properties of pectin hydrogels by starch addition. *Journal of Food Science and Technology, 58*, 302–310. https://doi.org/10.1007/s13197-020-04543-x

Bu, K. X., Huang, D. J., Li, D. P., & Zhu, C. H. (2022). Encapsulation and sustained release of curcumin by hawthorn pectin and Tenebrio Molitor protein composite hydrogel. *International Journal of Biological Macromolecules, 222*, 251–261. https://doi.org/10.1016/j.ijbiomac.2022.09.145

Bu, Q. Y., Chen, Y., Ding, Y., Zhang, K. X., Li, Y. C., You, X. Y., & Zhao, G. P. (2023). Preparation and characterization of tea polyphenol composite microspheres encapsulated using sodium alginate and crosslinked starch. *LWT-Food Science and Technology, 184*, 114888. https://doi.org/10.1016/j.lwt.2023.114888

Bušić, A., Belščak-Cvitanović, A., Cebin, A. V., Karlović, S., Kovač, V., Igor Špoljarić, Mršić, G., & Komes, D. (2018). Structuring new alginate network aimed for delivery of dandelion (*Taraxacum officinale* L.) polyphenols using ionic gelation and new filler materials. *Food Research International, 111*, 244–255. https://doi.org/10.1016/j.foodres.2018.05.034

Bhola, J., & Bhadekar, R. (2024). Prebiotic effect of daily dietary polyphenols and oligosaccharides on *lactobacillus* species. *Bioactive Carbohydrates and Dietary Fibre, 31*, 100407. https://doi.org/10.1016/j.bcdf.2024.100407

Cai, R., Pan, S. Y., Li, R. X., Xu, X. Y., Pan, S. Y., & Liu, F. X. (2022). Curcumin loading and colon release of pectin gel beads: Effect of different de-esterification

761 method. *Food Chemistry, 389*, 133130.
762 https://doi.org/10.1016/j.foodchem.2022.133130
763 Chan, E. S., Wong, S. L., Lee, P. P., Lee, J. S., Ti, T. B., Zhang, Z. B., Poncelet, D.,
764 Ravindra, P., Phan, S. H., & Yim, Z. H. (2011). Effects of starch filler on the
765 physical properties of lyophilized calcium-alginate beads and the viability of
766 encapsulated cells. *Carbohydrate Polymers, 83*, 225–232.
767 https://doi.org/10.1016/j.carbpol.2010.07.044
768 Chen, N., Feng, Z. J., Gao, H. X., He, Q., & Zeng, W. C. (2024). Core-shell structured
769 alginate-based hydrogel beads modified by starch and protocatechuic acid:
770 Preparation, characterization, phenolic slow release and stable antioxidant
771 potential. *Food Chemistry, 459*, 140389.
772 https://doi.org/10.1016/j.foodchem.2024.140389
773 Chen, L., Tong, Q. Y., Ren, F., & Zhu, G. L. (2014). Pasting and rheological properties
774 of rice starch as affected by pullulan. *International Journal of Biological*
775 *Macromolecules, 66*, 325–331. https://doi.org/10.1016/j.ijbiomac.2014.02.052
776 Cortés-Camargo, S., Román-Guerrero, A., Alvarez-Ramirez, J., Alpizar-Reyes, E.,
777 Velázquez-Gutiérrez, S. K., & Pérez-Alonso, C. (2023). Microstructural influence
778 on physical properties and release profiles of sesame oil encapsulated into sodium
779 alginate-tamarind mucilage hydrogel beads. *Carbohydrate Polymer Technologies*
780 *and Applications, 5*, 100302. https://doi.org/10.1016/j.carpta.2023.100302
781 Dahal, P., & Janaswamy, S. (2024). Hydrocolloid-based nutraceutical delivery systems:
782 Potential of κ-carrageenan hydrogel beads for sustained release of curcumin. *Food*
783 *Research International, 183*, 114223.
784 https://doi.org/10.1016/j.foodres.2024.114223
785 Dumitriu, R. P., Mitchell, G. R., & Vasile, C. (2011). Rheological and thermal behaviour
786 of poly (*N*-isopropylacrylamide)/alginate smart polymeric networks. *Polymer*
787 *International, 60*, 1398–1407. https://doi.org/10.1002/pi.3093
788 Feltrea, G., Almeidaa, F. S., Satoa, A. C. K., Dacanalb, G. C., & Hubinger, M. D. (2020).
789 Alginate and corn starch mixed gels: Effect of gelatinization and amylose content
790 on the properties and *in vitro* digestibility. *Food Research International, 132*,

109069. https://doi.org/10.1016/j.foodres.2020.109069

Günter, E. A., Martynov, V. V., Ananchenko, B. A., Martinson, E. A., Litvinets, S. G. (2022). The gel strength and swelling in the gastrointestinal environment of pectin/κ-carrageenan gel particles based on pectins with different degrees of methylesterification. *Materials Today Communications, 33*, 104986. https://doi.org/10.1016/j.mtcomm.2022.104986

Han, X. Y., Ma, P., Shen, M. Y., Wen, H. L., & Xie, J. H. (2023). Modified porous starches loading curcumin and improving the free radical scavenging ability and release properties of curcumin. *Food Research International, 168*, 112770. https://doi.org/10.1016/j.foodres.2023.112770

Hu, M., Du, X. Q., Liu, G. N., Huang, Y. Y., Qi, B. K., Li, Y. (2021). Sodium alginate/soybean protein-epigallocatechin-3-gallate conjugate hydrogel beads: evaluation of structural, physical, and functional properties. *Food & Function, 12*(24), 12347–12361. https://doi.org/10.1039/d1fo03099j

Jiang, B., Li, W., Hu, X., Wu, J., & Shen, Q. (2015). Rheology of mung bean starch treated by high hydrostatic pressure. *International Journal of Food Properties, 18*, 81–92. https://doi.org/10.1080/10942912.2013.819363

Jiang, X. Y., Li, L., Yan, J. N., Zhang, L. C., Wang, C., Lai, B., & Wu, H. T. (2024). Characterization of hydrogel beads constructed from gelatinized lotus rhizome starch and sodium alginate by calcium cross-linking. *Food Hydrocolloids, 154*, 110102. https://doi.org/10.1016/j.foodhyd.2024.110102

Jiang, X., Gu, Y., Zhang, L., Sun, J., Yan, J., & Wang, C. (2023). Physicochemical properties of granular and gelatinized lotus rhizome starch with varied proximate compositions and structural characteristics. *Foods, 12*(23), 4330. https://doi.org/10.3390/foods12234330

Lee, T., & Chang, Y. H. (2020). Structural, physicochemical, and in-vitro release properties of hydrogel beads produced by oligochitosan and de-esterified pectin from yuzu (Citrus junos) peel as a quercetin delivery system for colon target. *Food Hydrocolloids, 108*, 106086. https://doi.org/10.1016/j.foodhyd.2020.106086

Lee, Y. E., Kang, Y. R., & Chang, Y. H. (2023). Effect of pectic oligosaccharide on

probiotic survival and physicochemical properties of hydrogel beads for synbiotic encapsulation of *Lactobacillus bulgaricus*. *Food Bioscience, 51*, 102260. https://doi.org/10.1016/j.fbio.2022.102260

Lenie, M. D. R., Ahmadzadeh, S., Bockstaele, F. V., & Ubeyitogullari, A. (2024). Development of a pH-responsive system based on starch and alginate-pectin hydrogels using coaxial 3D food printing. *Food Hydrocolloids, 153*, 109989. https://doi.org/10.1016/j.foodhyd.2024.109989

Li, H., Gao, Z. X., Xu, J. J., Sun, W., Wu, J. R., Zhu, L., Gao, M. J., & Zhan, X. B. (2022). Encapsulation of polyphenols in pH-responsive micelles self-assembled from octenyl-succinylated curdlan oligosaccharide and its effect on the gut microbiota. *Colloids and Surfaces B: Biointerfaces, 219*, 112857. https://doi.org/10.1016/j.colsurfb.2022.112857

Li, Q., Duan, M. R., Hou, D., Chen, X. Q., Shi, J. L., & Zhou, W. (2021). Fabrication and characterization of Ca (II)-alginate-based beads combined with different polysaccharides as vehicles for delivery, release and storage of tea polyphenols. *Food Hydrocolloids, 112*, 106274. https://doi.org/10.1016/j.foodhyd.2020.106274

Li, Y. H., Zhang, C., Li, S. Y., Zhu, Z. Z., Wang, X. H., & Cravotto, G. (2024). Improving complexation of puerarin with kudzu starch by various ultrasonic pretreatment: Interaction mechanism analysis. *Ultrasonics Sonochemistry, 111*, 107095. https://doi.org/10.1016/j.ultsonch.2024.107095

Li, Z. X., Geng, Y. X., Bu, K. X., Chen, Z. T., Xu, K., & Zhu, C. H. (2024). Construction of a pectin/sodium alginate composite hydrogel delivery system for improving the bioaccessibility of phycocyanin. *International Journal of Biological Macromolecules, 269*, 131969. https://doi.org/10.1016/j.ijbiomac.2024.131969

Liu, R., Ci, X. M., Liu, L. L., Wang, X. T., Rifky, M., Liu, R., Sui, W. J., Wu, T., & Zhang, M. (2024). Chitosan entrapping of sodium alginate/Lycium barbarum polysaccharide gels for the encapsulation, protection and delivery of *Lactiplantibacillus plantarum* with enhanced viability. *International Journal of Biological Macromolecules, 260*, 129615. https://doi.org/10.1016/j.ijbiomac.2024.129615

Lopes, M. M., Oliveira-Paiva, C. A., & Farinas, C. S. (2023). Modification of pectin/starch-based beads with additives to improve *Bacillus subtilis* encapsulation for agricultural applications. *International Journal of Biological Macromolecules, 246*, 125646. https://doi.org/10.1016/j.ijbiomac.2023.125646

Lozano-Vazquez, G., Lobato-Calleros, C., Escalona-Buendia, H., Chavez, G., Alvarez-Ramirez, J., & Vernon-Carter, E. J. (2015). Effect of the weight ratio of alginate-modified tapioca starch on the physicochemical properties and release kinetics of chlorogenic acid containing beads. *Food Hydrocolloids, 48*, 301–311. https://doi.org/10.1016/j.foodhyd.2015.02.032

Lin, S. Y., Liu, X. E., Cao, Y., Liu, S. C., Deng, D. W., Zhang, J. S., & Huang, G. H. (2021). Effects of xanthan and konjac gums on pasting, rheology, microstructure, crystallinity and *in vitro* digestibility of mung bean resistant starch. *Food Chemistry, 339*, 128001. https://doi.org/10.1016/j.foodchem.2020.128001

Paswan, M., Chandel, A. K. S., Malek, N. I., & Dholakiya, B. Z. (2024). Preparation of sodium alginate/Cur-PLA hydrogel beads for curcumin encapsulation. *International Journal of Biological Macromolecules, 254*, 128005. https://doi.org/10.1016/j.ijbiomac.2023.128005

Qi, X. X., Simsek, S., & Chen, B. C. (2020). Alginate-based double-network hydrogel improves the viability of encapsulated probiotics during simulated sequential gastrointestinal digestion: Effect of biopolymer type and concentrations. *International Journal of Biological Macromolecules, 165*, 1675–1685. https://doi.org/10.1016/j.ijbiomac.2020.10.028

Qiu, Z. C., Li, L. Y., Zhu, W. Q., Qiao, X. G., Zheng, Z. J., & Sun-Waterhouse, D. X. (2024). Pectins rich in RG-I and galactose extracted from garlic pomace: Physicochemical, structural, emulsifying and antioxidant properties. *Food Hydrocolloids, 149*, 109559. https://doi.org/10.1016/j.foodhyd.2023.109559

Raza, H., Zhou, Q., Cheng, K. W., He, J. Y., & Wang, M. F. (2024). Synergistic impact of ultrasound-high pressure homogenization on the formation, structural properties, and slow digestion of the starch-phenolic acid complex. *Food Chemistry, 445*, 138785. https://doi.org/10.1016/j.foodchem.2024.138785

Razavi, S., Janfaza, S., Tasnim, N., Gibson, D. L., & Hoorfar, M. (2021). Microencapsulating polymers for probiotics delivery systems: Preparation, characterization, and applications. *Food Hydrocolloids, 120*, 106882. https://doi.org/10.1016/j.foodhyd.2021.106882

Reichembach, L. H., Petkowicz, C. L. O., Guerrero, P., & Caba, K. (2024). Pectin and pectin/chitosan hydrogel beads as coffee essential oils carrier systems. *Food Hydrocolloids, 151*, 109814. https://doi.org/10.1016/j.foodhyd.2024.109814

Ren, Y. M., Jiang, L., Wang, W. J., Xiao, Y. H., Liu, S. C., Luo, Y., Shen, M. Y., & Xie, J. H. (2020). Effects of Mesona chinensis Benth polysaccharide on physicochemical and rheological properties of sweet potato starch and its interactions. *Food Hydrocolloids, 99*, 105371. https://doi.org/10.1016/j.foodhyd.2019.105371

Ren, Y. M., Rong, L. Y., Shen, M. Y., Liu, W. M., Xiao, W. H., Luo, Y., & Xie, J. H. (2020). Interaction between rice starch and Mesona chinensis Benth polysaccharide gels: Pasting and gelling properties. *Carbohydrate Polymers, 240*, 116316. https://doi.org/10.1016/j.carbpol.2020.116316

Rohman, S., Kaewtatip, K., Kantachote, D., & Tantirungkij, M. (2021). Encapsulation of *Rhodopseudomonas palustris* KTSSR54 using beads from alginate/starch blends. *Journal of Applied Polymer Science, 138*, 50084. https://doi.org/10.1002/app.50084

Sarkar, S., Manna, S., Das, E., Jana, P., Mukherjee, S., Sahu, R., Dua, T. K., Paul, P., Kaity, S., & Nandi, G. (2024). Fabrication and optimization of extended-release beads of diclofenac sodium based on Ca^{2+} cross-linked Taro (*Colocasia esculenta*) stolon polysaccharide and pectin by quality-by-design approach. *International Journal of Biological Macromolecules, 271*, 132606. https://doi.org/10.1016/j.ijbiomac.2024.132606

Silveira, M. P., Almeida, F. L. C., Andreola, K., Alvim, I. D., & Prata, A. S. (2023). Influence of composition on the internal diffusion mechanism of pectin-starch gel beads. *Journal of Applied Polymer Science, 140*(9), E53570. https://doi.org/10.1002/app.53570

911 Singh, P., Medronho, B., Alves, L., Silva, G.J., Miguel, M.G., Lindman, B. (2017).
912 Development of carboxymethyl cellulose-chitosan hybrid micro- and
913 macroparticles for encapsulation of probiotic bacteria. *Carbohydrate Polymers,*
914 *175*, 87–95. https://doi.org/10.1016/j.carbpol.2017.06.119
915 Su, C. Y, Xia, T., Li, D., Wang, L. J, & Wang, Y. (2023). Hybrid biodegradable materials
916 from starch and hydrocolloid: fabrication, properties and applications of starch-
917 hydrocolloid film, gel and bead. *Critical Reviews in Food Science and Nutrition*,
918 *64*(33), 12841–12859. https://doi.org/10.1080/10408398.2023.2257786
919 Sun, W. X., Bu, K. X., Meng, H. M., & Zhu, C. H. (2024). Hawthorn pectin/soybean
920 isolate protein hydrogel bead as a promising ferrous ion-embedded delivery
921 system. *Colloids and Surfaces B: Biointerfaces, 237*, 113867.
922 https://doi.org/10.1016/j.colsurfb.2024.113867
923 Ubeyitogullari, A., & Ciftci, O. N. (2016). Formation of nanoporous aerogels from
924 wheat starch. *Carbohydrate Polymers, 147*, 125–132.
925 https://doi.org/10.1016/j.carbpol.2016.03.086
926 Ubeyitogullari, A., & Ciftci, O. N. (2019). A novel and green nanoparticle formation
927 approach to forming low-crystallinity curcumin nanoparticles to improve
928 curcumin's bioaccessibility. *Scientific Reports, 9*, 19112.
929 https://doi.org/10.1038/s41598-019-55619-4
930 Vaziri, A. S., Alemzadeh, I., Vossoughi, M., & Khorasani, A. C. (2018). Co-
931 microencapsulation of *Lactobacillus plantarum* and DHA fatty acid in alginate-
932 pectin-gelatin biocomposites. *Carbohydrate Polymers, 199*, 266–275.
933 https://doi.org/10.1016/j.carbpol.2018.07.002
934 Wang, H., Yang, L., Yang, Y. N., Zhang, D. S., & Hao, G. L. (2025). Multifunctional
935 natural starch-based hydrogels: Critical characteristics, formation mechanisms,
936 various applications, future perspectives. *Carbohydrate Polymers*, *357*, 123458.
937 https://doi.org/10.1016/j.carbpol.2025.123458
938 Wan, L., Yang, Z. X., Cai, R., Pan, S. Y., Liu, F. X., & Pan, S. Y. (2021). Calcium-
939 induced-gel properties for low methoxyl pectin in the presence of different sugar
940 alcohols. *Food Hydrocolloids, 112*, 106252.

https://doi.org/10.1016/j.foodhyd.2020.106252

Wang, S. J., Wu, Z. N., Jia, L. Y., Wang, X. H., He, T., Wang, L., Yao, G. J., & Xie, F. Y. (2024). Soybean protein isolate-sodium alginate double network emulsion gels: Mechanism of formation and improved freeze-thaw stability. *International Journal of Biological Macromolecules, 274*, 133296. https://doi.org/10.1016/j.ijbiomac.2024.133296

Wang, W. J., Shen, M. Y., Liu, S. C., Jiang, L., Song, Q. Q., & Xie, J. H. (2018). Gel properties and interactions of *Mesona blumes* polysaccharide-soy protein isolates mixed gel: The effect of salt addition. *Carbohydrate Polymers, 192*, 193–201. https://doi.org/10.1016/j.carbpol.2018.03.064

Wang, X. W., Feng, Y. W., & Feng, T. T. (2021). Modulation effect of glycerol on plasticization and water distribution of vacuum-dried calcium alginate gel beads encapsulating peppermint oil/*β*-cyclodextrin complex. *Food Bioscience, 41*, 100968. https://doi.org/10.1016/j.fbio.2021.100968

Xiao, W. H., Shen, M. Y., Li, J. W., Li, Y. L., Qi, X., Rong, L. Y., Liu, W. M., & Xie, J. H. (2023). Preparation and characterization of curcumin-loaded debranched starch/*Mesona chinensis* polysaccharide microcapsules: Loading levels and in vitro release. *Food Hydrocolloids, 141*, 108697. https://doi.org/10.1016/j.foodhyd.2023.108697

Xiao, W. H., Shen, M. Y., Ren, Y. M., Wen, H. L., Li, J. W., Rong, L. Y., Liu, W. M., & Xie, J. H. (2022). Controlling the pasting, rheological, gel, and structural properties of corn starch by incorporation of debranched waxy corn starch. *Food Hydrocolloids, 123*, 107136. https://doi.org/10.1016/j.foodhyd.2021.107136

Yang, J. Y., Song, J. L., Miao, S., Gao, Y. X., & Mao, L. K. (2024). Alginate-based gel beads with bigel structures: Preparation, characterization and bioactive encapsulation. *Food Hydrocolloids, 146*, 109294. https://doi.org/10.1016/j.foodhyd.2023.109294

Ye, J. P., Yang, R., Liu, C. M., Luo, S. J., Chen, J., Hu, X. T., & Wu, J. Y. (2018). Improvement in freeze-thaw stability of rice starch gel by inulin and its mechanism. *Food Chemistry, 268*, 324–333. https://doi.org/10.1016/j.foodchem.2018.06.086

971 Zhu, W. Q., Bai, X. Y., Du, W. B., Li, L. Y., Fauconnier, M. L., Richel, A., Dong, H. J.,
972 & Zheng, Z. J. (2025). Comparison of the properties of turmeric starch-dioscin-
973 curcumin nanocarriers prepared by antisolvent co-precipitation and antisolvent
974 precipitation. *Carbohydrate Polymers, 353*, 123263.
975 https://doi.org/10.1016/j.carbpol.2025.123263
976 Zhang, F., Zheng, X. J., Ma, Y., Nan, W. Q., Wu, W. J., Chu, Z. R., Sun, X., Huang, J.
977 H., Muratkhan, M., Yue, F. F., Wang, X., & Lv, X. (2025). Sodium alginate/low
978 methoxyl pectin composite hydrogel beads prepared via gas-shearing technology
979 for enhancing the colon-targeted delivery of probiotics and modulating gut
980 microbiota. *International Journal of Biological Macromolecules, 300*, 140375.
981 https://doi.org/10.1016/j.ijbiomac.2025.140375
982 Zhang, Y., Zhao, T., Ma, & X. R. (2025). Innovative modified pectins enriched with
983 galactose: Preparation, characterization, and gel-based properties of curcumin-
984 delivered hydrogel beads. *Food Hydrocolloids, 2025*, 160, 110757.
985 https://doi.org/10.1016/j.foodhyd.2024.110757
986 Zhang, Y., Zhao, X. T., Bao, X. Y., Xiao, J., & Liu, H. S. (2021). Effects of pectin and
987 heat-moisture treatment on structural characteristics and physicochemical
988 properties of corn starch. *Food Hydrocolloids, 117*, 106664.
989 https://doi.org/10.1016/j.foodhyd.2021.106664

Figure captions

Fig. 1. Visual appearance of PP@GB, TS@GB, TSNC@GB, MTSNC@GB, and TS-CUR@GB gel beads.

Fig. 2. FTIR spectra (A) and XRD patterns (B) of PP@GB, TS@GB, TSNC@GB, MTSNC@GB, and TS-CUR@GB gel beads.

Fig. 3. TGA curves (A) and DTG curves (B) of PP@GB, TS@GB, TSNC@GB, MTSNC@GB, and TS-CUR@GB gel beads.

Fig. 4. SEM images of PP@GB, TS@GB, TSNC@GB, MTSNC@GB, and TS-CUR@GB gel beads.

Fig. 5. Water holding capacity (A), swelling behavior (B), and water distribution profiles (C) of PP@GB, TS@GB, TSNC@GB, MTSNC@GB, and TS-CUR@GB gel beads. Different lowercase letters indicate significant differences ($P<0.05$).

Fig. 6. Dynamic modulus variation curves (A) and shear viscosity variation curves (B) of PP@GB, TS@GB, TSNC@GB, MTSNC@GB, and TS-CUR@GB gel beads.

Fig. 7. Texture properties of PP@GB, TS@GB, TSNC@GB, MTSNC@GB, and TS-CUR@GB gel beads. Different lowercase letters indicate significant differences ($P<0.05$).

Fig. 8. Colonization of *Lactiplantibacillus plantarum* Lp3a at a concentration of 10^{-6} after different sample treatments (A): Blank (a), PP@GB (b), TS@GB (c), TSNC@GB (d), MTSNC@GB (e), and TS-CUR@GB (f). Effect of different samples on the proliferation of *Lactiplantibacillus plantarum* Lp3a (B). Different lowercase letters indicate significant differences ($P<0.05$).

- Pectin-starch composite gel beads were successfully fabricated by ion cross-linking
- Starch derivatives enhanced the structural integrity and texture properties of gel beads
- Starch derivatives improved the swelling behavior and thermal stability of gel beads
- Curcumin and pectin synergistically enhance the prebiotic activity of TS-CUR@GB
- Curcumin-enriched starch fillers exhibited superior modification effects

Declaration of interest statement

The authors declare that they have no known competing financial interests or personal relationships that could have appeared to influence the work reported in this paper.